NASA TECHNICAL MEMORANDUM

NASA TM X-73662

NASA TM X-73662

AERO-ACOUSTIC PERFORMANCE COMPARISON OF CORE ENGINE NOISE SUPPRESSORS ON NASA QUIET ENGINE "C"

by Harry E. Bloomer and John W. Schaefer
Lewis Research Center
Cleveland, Ohio 44135

TECHNICAL PAPER to be presented at the
Thirteenth Propulsion Conference
cosponsored by the American Institute of Aeronautics
and Astronautics and the Society of Automotive Engineers
Orlando, Florida, July 11-13, 1977

AERO-ACOUSTIC PERFORMANCE COMPARISON OF CORE ENGINE NOISE SUPPRESSORS ON NASA QUIET ENGINE "C"

Harry E. Bloomer and John W. Schaefer

National Aeronautics and Space Administration
Lewis Research Center
Cleveland, Ohio 44135

E-9182

Abstract

The purpose of the experimental program reported herein was to evaluate and compare the relative aero-acoustic effectiveness of two core engine suppressors, a contractor-designed suppressor delivered with the Quiet Engine, and a NASA-designed suppressor, designed and built subsequently. The NASA suppressor was tested with and without a splitter making a total of three configurations being reported in addition to the baseline hardwall case. The aerodynamic results are presented in terms of tailpipe pressure loss, corrected net thrust, and corrected specific fuel consumption as functions of engine power setting. The acoustic results are divided into duct and far-field acoustic data. The NASA-designed core suppressor did the better job of suppressing aft end noise, but the splitter associated with it caused a significant engine performance penalty. The NASA core suppressor without the splitter suppressed most of the core noise without any engine performance penalty.

Introduction

To achieve core engine noise suppression for the approach flight condition of a typical CTOL mission, many types of suppressors have been proposed. The purpose of the experimental program reported herein was to evaluate and compare the relative aero-acoustic effectiveness of two core engine suppressors, a contractor-designed suppressor delivered with the Quiet Engine, and a NASA-designed suppressor, designed and built subsequently. The NASA suppressor was tested with and without a splitter making a total of three configurations being reported in addition to the baseline hardwall case.

As a part of the NASA Quiet Engine contractor program, a core suppressor was designed and tested on Quiet Engine "C". The design was aimed mainly at suppression of turbine noise at approach power and its attenuation characteristic was centered at a frequency of 5000 Hertz. The mechanical design was selected in consideration of types of acoustic materials available, methods of fabrication, and duty cycles required. This information was presented in Refs. 1 and 2. The performance of this configuration was reported in Refs. 2 and 3 and showed that the totally suppressed engine was aft-end noise dominated over the range of engine power settings.

In an effort to provide a greater suppression of the core noise, a second suppressor was designed having upstream and downstream sections, each designed for different frequencies. Single degree of freedom (SDOF) treatment was used in each section. The second suppressor incorporated a tailpipe splitter to improve the suppression at a frequency of 6300 Hz centered around the turbine tones. The second section of treatment was designed for 2500 Hz (much lower than the lowest frequency turbine tones), to suppress other broadband noise emanating from the core. The splitter was designed so that it could be removed, resulting in a third configuration to be evaluated.

The three configurations, the contractor design and the NASA design with and without the splitter, were evaluated aero-acoustically on Quiet Engine "C" at the Engine Noise Test Facility of NASA Lewis Research Center. The core suppressor configurations were tested over a range of engine power settings from approach to takeoff. Fan noise was suppressed forward by a sonic inlet described in Ref. 4 in its takeoff configuration, and aft by a massive aft fan suppressor[3] so that the aft core noise could be measured. A coplanar fan and core nozzle arrangement was installed to minimize the turbulent mixing zone between the fan and core jets resulting in a reduction in the jet exhaust sound scattering[5] and also to minimize "haystacking"[6]. This permitted the better discrimination of the various turbine tones and consequently allowed the noise reduction of the core suppressor to be measured more accurately in the far field. Aerodynamic performance tests as well as both far-field and duct acoustic tests were performed and results are compared herein to baseline test results of the engine with no core acoustic treatment. Results from the acoustic suppression prediction method of Ref. 7 are compared with the experimental results.

Apparatus and Procedure

Facility Description

The test program was performed at the Engine Noise Test Facility located at Lewis Research Center adjacent to, but sufficiently far from the Flight Research Building so that accurate acoustic measurements could be obtained. The facility is shown schematically in Fig. 1.

The 17 far-field microphones were at the same height as the engine centerline, 3.96 m (13 ft), on a 45.7-m (150-ft) radius spaced every 10° from the inlet axis to 160°. The reflecting plane was hard pavement. Ground microphones were installed at 110°, 120°, 130°, and 140° from the inlet axis.

A photograph showing the installation of Quiet Engine "C" at the Engine Noise Test Facility is presented in Fig. 2. Engine operation was controlled from the Flight Research Building where the noise instrumentation and analysis equipment were located.

Engine Description

The NASA Quiet Engine "C", a low noise technology turbofan demonstrator, was designed, built, and acoustically evaluated under the NASA/GE Experimental Quiet Engine Program. The 97,900-newton (22,000-lb) thrust class turbofan consisted of a newly developed, high tip speed, single-stage fan. It was designed for the altitude cruise condition with a corrected tip speed of 472 m/sec (1550 ft/sec) at a bypass pressure ratio of 1.6, and with a corrected fan flow of 415 kg/sec (915 lb/sec). The

STAR Category 07

fan had 26 unshrouded rotor blades and 60 outlet guide vanes. Further details are presented in Ref. 3.

Core Suppressor Design

A schematic of the contractor-designed core suppressor (hereafter referred to as configuration 1) is presented in Fig. 3. The acoustic treatment was of the SDOF type with a 7% porosity face plate and a total thickness of 0.64 cm (0.25 in.). The face plate had a thickness of 0.508 mm (0.020 in.).

A schematic of the NASA designed core suppressor (hereafter referred to as configuration 2) is presented in Fig. 4(a) and a photograph is shown in Fig. 4(b). The instrumentation shown is discussed in the "Experimental Methods" section of this report. Two sections of treatment with two thicknesses were provided with a splitter in the upstream, high frequency section. The splitter reduced the frequency parameter, fH/c, and increased the average length to height ratio, L/H, both of which increased the effectiveness of the treatment in that section. The splitter was removable so that the performance penalty/noise suppression tradeoff could be measured. It was realized that the splitter used in this design might cause more pressure drop than would be desirable necessitating a new tailpipe design. However, a new tailpipe design was not considered economical for this demonstration test. The configuration with the splitter removed will hereafter be referred to as configuration 3.

The design goal for configuration 2 was determined from the NOY-weighted baseline spectrum data at engine approach power obtained by the contractor in his tests of Engine "C". These data are presented in Fig. 5. The assumption was made that all the NOY-weighted spectrum measured at 120° in the far field above a level of 68 dB was emanating from the core. By suppressing the NOY-weighted spectrum down to a level of about 68 dB, it was hoped that essentially all of the turbine and other core noise above a frequency of 500 Hz could be effectively eliminated. With this goal in mind, many acoustic liner designs were analyzed in an effort to reach the suppression required. The acoustic liner design method described in Ref. 7 along with the design constraints of not extending the tailpipe resulted in a design which incorporated a splitter in the high frequency section. Another constraint imposed by the hardware can be seen in Fig. 4(a). The downstream end of the low frequency section had no treatment on the outside wall because no room existed for the thick treatment. The result was that the last 19 cm (7.5 in.) of treatment on the tailcone had a very large average effective passage height of 58 cm (23 in.), which was two times the average passage height of 29 cm. For the high frequency treatment, an average length of only 21.9 cm (8.6 in.) in the outer passage had like treatment opposite. With the splitter removed, the average L/H value for the high frequency section of treatment decreased from 2.42 to 1.09.

The predicted acoustic suppression of the configurations using the method of Ref. 7, along with the design goal for configuration 2 are presented in Fig. 6. The design center frequency of suppression for configuration 1 was 5000 Hz. The two types of treatment employed in configurations 2 and 3 had design center frequencies of 2500 and 6300 Hz. The effect of removing the splitter causes a drastic reduction in predicted suppression from 20.3 to 5.6 dB at a frequency of 6300 Hertz. The predicted reduction at 2500 Hertz also drops from 16 to 10 dB. This is because the "skirt" of off-peak attenuation of the high frequency treatment also drops when the peak attenuation drops at 6300 Hertz. The off-peak attenuation or "skirt" of configuration 1 has a flatter slope than the other configurations. This characteristic is caused by the prediction program which treats configuration 1 as an "overdamped" liner. Overdamping occurs when the resistance ratio (θ/θ_{opt}) exceeds unity.

The aerodynamic design of the splitter used in configuration 2 was carefully considered to minimize any additional tailpipe pressure loss. A potential flow analysis was used and wall curvature of the leading edge of the splitter was designed to minimize the possibility of separation over the range of engine flow conditions. Additional design details are presented in Appendix A.

The mechanical design of configuration 2 also entailed some problems in consideration of the effects of the engine environment on the suppressor structure. These are treated in some detail in Appendix B.

Fully Suppressed Engine Configuration

The fully suppressed engine configuration employed in these tests is shown schematically in Fig. 7. Details of the acoustic treatment in the inlet and aft fan ducts are also shown. The acoustic performance of this configuration was reported in Ref. 4. Shown also in Fig. 7 is the co-planar nozzle extension which was used for the majority of the tests.

Experimental Methods

Aerodynamic and acoustic data were obtained over a range of corrected fan speeds from 55 to 93 percent of design for all three core suppressor configurations and the hardwall baseline configuration.

The acoustic instrumentation and data recording system had a flat response over the frequency range of interest (50 to 20,000 Hz). Data signals were FM recorded from all channels simultaneously on magnetic tape. Each of the three samples for a given corrected fan speed was reduced separately by using a 1/3-octave-band analyzer. The resulting sound pressure levels were arithmetically averaged, adjusted to standard day atmospheric conditions; and side-line perceived noise levels were calculated using the standardized procedures presented in Ref. 8. The narrow band data reported herein are given as measured without any correction.

Aerodynamic instrumentation was located in planes identified in Fig. 8. The total pressures and temperatures at the turbine outlet and the core nozzle outlet stations were located on centers of equal flow areas. The spacing of the total pressures measured at the splitter station is indicated in Fig. 9. The pressures, temperatures, and other outputs were received as millivolt signals by the facility data system, digitized and transmitted from a local minicomputer to a remote data collector at the laboratory main computer facility. A laboratory computer then reduced the data to appropriate aerodynamic parameters. Thrust was measured with a load cell and corrected in the following

manner. The axial component of the wind velocity into the inlet was multiplied by the engine mass flow and divided by the gravitational constant. The resulting term was added to the thrust measured by the load cell. No thrust correction was made for winds coming from the rear quadrants of the engine.

In-duct acoustic data were obtained using traversing probes at the core nozzle outlet station (fig. 8). These area-weighted data measured downstream of the core suppressor treatment were subtracted from similar acoustic probe data obtained from the baseline configuration (with no acoustic treatment) to yield (PWL) sound power level reduction in each 1/3-octave band.

Flyover noise time histories were calculated for a constant airplane altitude and using each far-field microphone reading extrapolated to the proper distance and adjusted for the number of engines assumed. (In this case four, assuming a B707/DC8 type airplane. The altitude assumed for the approach flyover was 114 m (375 ft).)

Results and Discussion

The aerodynamic results are presented in terms of tailpipe pressure loss, corrected net thrust, and corrected specific fuel consumption as functions of corrected fan speed.

The acoustic results are divided into duct and far-field acoustic data. The duct data are displayed as PWL sound power level reduction across the tailpipe treatment as a function of frequency for approach and takeoff power settings. The far-field acoustic data at both approach and takeoff power settings are shown as functions of sideline perceived noise level (PNL) directivities. Detailed 1/3-octave band and narrowband spectra are presented for the 120° peak noise aft angle for the approach power setting. A comparison of the predicted noise reduction of the core suppressors to the duct results and the far-field results is then discussed. Finally, time histories of tone corrected perceived noise levels (PNLT's) are shown for the configurations at the approach flight condition.

Aerodynamic Performance

Typical total-to-static pressure ratio profiles at the turbine outlet station for both approach and takeoff power settings are presented in Fig. 9. Pressure ratio is shown as a function of percent of total annulus area measured from the outside to the inside wall. At both approach and takeoff power, the pressure ratio peaks at the center and falls off more toward the inner wall than the outer wall.

Typical pressure ratio profiles obtained at the splitter outlet station for both approach and takeoff power settings are presented in Fig. 10. Total-to-static pressure ratio behind the splitter is shown as a function of distance from the centerline of the splitter. At approach power, the pressure ratio in the outside flow passage drops from a value of about 1.06 to 1.02 at the centerline. The inside passage average pressure ratio is slightly lower than 1.06 (about 1.05). This agrees with the trend at the turbine outlet (previous figure) which showed a lower velocity in the inner flow passage. At takeoff power, the inside and outside passage average pressure ratios are about 1.16 and the splitter centerline pressure ratio drops to 1.04. The splitter boundary layer thickness is not excessive (about 1 cm), and the profile is reasonably smooth indicating no flow separation. The splitter was designed to split the flow evenly at takeoff power and seems to be doing just that.

Presented in Fig. 11(a) is a comparison of tailpipe pressure loss factor, $(P_{T,5.6} - P_{T,8.0})/P_{T,5.6}$, as a function of corrected core engine speed for configurations 2 and 3. These configurations, the NASA design with and without the splitter, have a total pressure loss factor of 0.015 at approach power. The turbine outlet flow Mach number is low (about 0.27)(fig. 11(c)) and the swirl angle is high (about 13°)(fig. 11(b)). At a corrected core speed of 8300 rpm, the swirl angle has decreased and the effect of the small increase in flow Mach number (up to about 0.3) has not yet caused an increase in total pressure loss, so the pressure loss curve has a "valley" (about 0.014). As core speed is increased further to takeoff power, the increased flow Mach number (about 0.50) causes an increase in pressure loss. At takeoff power, the splitter of configuration 2 causes an increase from the total pressure loss factor of configuration 3 of 0.020 to about 0.026, an increase of 30 percent. These pressure loss data are considerably higher than those losses estimated by the engine contractor for configuration 2.

A comparison of corrected net thrust as a function of corrected fan speed is presented in Fig. 12 for the baseline and the three suppressor configurations. The baseline and configurations 1 and 3 data fall on essentially one line. The penalty for the splitter installation of configuration 2 is readily apparent. At takeoff rating, the penalty amounts to a decrement in corrected net thrust of about 4 percent. A more significant concern, however, is the effect of configuration changes on specific fuel consumption. This effect is illustrated next in Fig. 13. Corrected specific fuel consumption (SFC) is plotted as a function of corrected net thrust. Again the penalty for the splitter installation is apparent. The penalty in increased SFC at takeoff amounts to about 6 percent.

The effects of the splitter installation on Quiet Engine "C" performance is somewhat amplified by the use of the sonic inlet which is used to minimize front radiated fan noise. The somewhat lower inlet recovery produced by the sonic inlet in comparison to a conventional inlet[4] causes an increase in corrected SFC as corrected thrust is increased beyond 75 percent of takeoff power (fig. 13), and also causes the decrease in slope of corrected thrust as a function of corrected fan speed (fig. 12). It is estimated that at takeoff power the penalty in corrected SFC would be reduced from about 6 percent to 4-1/2 percent if a conventional inlet has been utilized in this investigation.

The loses associated with the splitter could be minimized in any new engine development by designing a new tailpipe to accommodate the splitter. The splitter blocks approximately 9 percent of the flow area and raises the surface Mach number around the nose of the splitter at takeoff to about 0.57. A somewhat flatter turbine outlet flow profile and less swirl (both, of course, functions of engine design) would also help reduce the losses reported herein. Placement of the splitter downstream in a larger flow cross-section area would also reduce

the aerodynamic losses. However, this would also result in a lower noise reduction, according to the acoustic design prediction method.

Acoustic Performance

Duct sound power level reduction. - The duct microphone data which was taken with the baseline and all three suppressor configurations is summarized in Fig. 14. Sound power level reduction in dB is shown as a function of 1/3-octave-band frequency for the three configurations for both approach (fig. 14(a)) and takeoff (fig. 14(b)) power settings. As expected, at the approach power setting, configuration 2 suppresses core noise over a wide band of frequency. The 2500-Hz 1/3-octave band is suppressed 10 dB and the 6300 Hz band is suppressed 13.5 dB. Even the 1000-Hz band is suppressed by 6 dB and the 20,000 Hz band by 4.5 dB. In contrast with this performance, configurations 1 and 3 have peak suppression values of about 7 dB at the 4000 Hz band. As would be expected, of the two configurations, configuration 3 has better suppression in the lower frequency bands and configuration 1 has better suppression in the higher frequency bands. At takeoff power setting, configuration 2 also provides reasonable suppression over the entire bandwidth presented, with peak suppression of 12.5 at 10,000 Hz. Configurations 1 and 3 also show peak suppressions at 10,000 Hz of 10.5 and 6.5 dB, respectively. The PWL reductions achieved by the three configurations at takeoff are lower than those at approach. The acoustic design point was at approach power so that the flow conditions are nonoptimum at takeoff. A second reason for the lower PWL reduction at takeoff, however, is that a jet noise floor has been reached. This will be discussed in some detail later in connection with the far-field acoustic results.

Farfield sound pressure level reductions. - The far-field PNL directivity data on a sideline are presented in Figs. 15 and 16 for approach and takeoff power settings, respectively. The approach power data are shown on a 114-m (375-ft) sideline as a function of angle from the engine inlet. The baseline noise peaks at angles of 50° and 120° from the inlet. Configuration 2 reduces the baseline noise by about 3.0 PNdB at 50° and 7.5 PNdB at 120°. Configuration 3 reduces the noise about the same amount as configuration 2 over the entire range of angles. Configuration 1 reduces aft quadrant noise about half as well as the other two configurations but does little in the front quadrant. The behavior of configurations 2 and 3 makes one suspect that a noise floor has been reached. At any rate, the engine equipped with either configuration 2 or 3 is no longer aft-noise dominated at approach power.

The PNL data at takeoff power are shown in Fig. 16 for a 305-m sideline as a function of angle from the engine inlet. In addition, jet noise calculated by the method of Ref. 9 is shown for comparison. The reductions in noise by all three configurations are small in comparison to the reductions at approach power. The aft peak of the baseline configuration noise at 120° is reduced by about 2 dB by configurations 2 and 3. The reductions at the other angles are also small. The reason is obvious when the jet noise floor is taken into account.

Shown in Fig. 17 is a comparison of 120° aft angle 305-m sideline PNL values for the baseline and three suppressor configurations as a function of corrected fan speed. The calculated jet noise is shown for reference. The estimated aft fan noise floor is also shown. The trends at approach and takeoff power settings have already been discussed in connection with Figs. 15 and 16. The trends at approach and takeoff are confirmed by the data points at 55 and 75 percent corrected design fan speed. Configuration 3 provides about the same amount of suppression as configuration 2 over the range of engine power settings tested. It appears that aft fan noise and jet noise are limiting the apparent reduction achieved by configuration 2 at takeoff and that aft fan noise alone constitutes a floor at approach.

In order to appraise the suppressor configurations on the basis of suppression of 1/3-octave-band noise, Fig. 18 is presented. These sound pressure level (SPL) data are for the 120° microphone at approach power setting extrapolated to a 114-m sideline. At frequencies between 1000 and 4000 Hz, configurations 2 and 3 suppress aft core noise equally well. At frequencies above 4000 Hz configuration 2 shows the greatest suppression. Configuration 1 does not accomplish much suppression at all frequencies in comparison to the others.

To further detail the comparison of these suppressors at approach power setting, far-field 120° microphone narrow band SPL data are presented in Fig. 19 over a range of 10,000 Hz. Shown in Fig. 19(a) is the baseline spectrum. The first and second stage low pressure (LP) turbine blade passing frequency (BPF) tones are readily apparent at frequencies of 6550 and 7200 Hz. This spectrum is repeated on Figs. 19(b), (c), and (d) so that the suppression of the configurations over the range of frequencies (10,000 Hz) can be noted. Displayed in Fig. 19(b) is the spectrum from configuration 2 showing the effect of nozzle configuration on far-field noise. As was reported in Ref. 3 and as predicted in Ref. 6, the spectrum of the standard fan nozzle (dashed) shows that "haystacking" did occur between the fan harmonic tones at 5950 Hz and the turbine tones emerging from the core. On the other hand, the coplanar nozzle configuration narrow band spectrum does contain clearly defined tones. The PNL for both configurations added up to about the same level, however. The second stage turbine tone for the coplanar nozzle is of higher amplitude than the tone for the standard fan nozzle, as reported in Ref. 3. It is reasonable that the turbine tones emanating from the core nozzle are modulated by the relatively larger eddies caused by the flow around the core nozzle when the fan nozzle is short compared to very small eddies with a coplanar nozzle.

A comparison of the splitterless configurations is presented in Fig. 19(c). Configuration 3 suppresses the noise better at frequencies between 1500 and 3900 and also suppresses the tones somewhat more than configuration 1. The frequencies between 3900 and 5400 Hz is the only range where configuration 1 is better.

A comparison of configurations 2 and 3 is presented in Fig. 19(d) to show the effect of the splitter. The two turbine tones were reduced by about 5 dB by the splitter. The SPL over the frequency range between 4500 and 7400 shows greater suppression by configuration 2. A close examination of the traces of configuration 2 shows that the fan BPF and first two harmonics are starting to appear in the narrow band data at a level above all other noise

except for the second stage turbine tone. This would suggest that, since the sound power contained in that tone on a PNL basis is very small, the noise floor is caused by the fan. In addition, the reduction in broadband noise at frequencies above 4500 Hz by configuration 2 means very little. Referring to Fig. 17 at low power settings, the greater suppression achieved by configuration 2 cannot be measured on a PNL basis.

At takeoff power setting, the picture is similar. Presented in Fig. 20 is a narrowband plot of SPL. The fan BPF and first harmonic tones are above the LP turbine first stage BPF tone. In addition, the low frequency jet noise, determined according to Ref. 9, is also starting to become dominant. The noise floor has been reached and the good suppression at frequencies beyond 6000 Hz means little in terms of PNL as shown in Fig. 17 at takeoff power setting. Since the PNL directivity shown in Fig. 16 is aft dominated, it is obvious that jet noise and aft fan noise are causing the floor.

Comparison with predictions. - In order to consider the accuracy of the prediction method[7], sound pressure level reductions measured in the core duct and in the far field at 120° angle from the inlet are presented as a function of 1/3-octave-band frequency in Fig. 21 for all three suppressor configurations at the approach power design point. Configuration 1 sound pressure level reduction shown in Fig. 21(a) shows relatively good agreement between the far-field and in-duct measurements. The pure tone reductions taken from narrowbands of Fig. 19 are also shown by the tailed symbols. The prediction overestimates the reduction over the frequency bandwidth. The discussion in the "Core Suppressor Design" section of the report should be recalled at this point. The fact that the configuration 1 liner is treated as "overdamped" according to the prediction method causes the broad "skirt" of the prediction curve. Perhaps, since this prediction is based on semiempiricism, these empirical data should be considered for a possible modification of the design method for the "overdamped" case.

Shown in Fig. 21(b) are the data for configuration 2. In addition, an estimate of the aft fan noise floor is shown based on Fig. 19(b). Here, relatively good agreement exists between both kinds of measurements and the prediction method. Even the peak suppression predicted at 6300 Hz is confirmed by the far-field data. The predicted peak suppression at 2500 Hz is not confirmed, due to the aforementioned fan noise floor at this frequency (fig. 19(b)).

Presented in Fig. 21(c) are the data for configuration 3. The same aft fan noise floor from Fig. 21(b) is also shown. The agreement between the measurements and the prediction is not as good as that shown in Fig. 21(b). The far-field suppression data, in fact, exceed the predicted suppression results and the measured in-duct suppression in the frequency range from 1600 to 4000 Hz and in the 1/3-octave bands of 6300 and 8000 Hz. A conclusion from the data presented in Fig. 21 is that the prediction method of Ref. 7 is a useful tool, but that improvements for off-optimum (overdamped) liner cases should be considered.

Effect on flyover noise. - A comparison of the approach time histories of tone corrected perceived noise levels (PNLT's), of the various configurations are presented in Fig. 22. These data were calculated from the far-field measured noise data assuming a four-engine B707/DC8 type of approach with an altitude of 114 m (375 ft) over the observer's station. Effective Perceived Noise Levels (EPNL's) are also shown for each time history in terms of Effective Perceived Noise decibels (EPNdB's).

Recall that the jet noise does not constitute a noise floor at this power setting, and therefore, no relative velocity corrections were needed in the calculation. Very little reduction in PNLT, and therefore, EPNdB was accomplished by configuration 1. Configurations 2 and 3 both show good reductions in PNLT equivalent to reductions of 2 and 3 EPNdB. Here, the fan noise floor apparently limits the reduction of EPNdB. Even though configuration 2 exhibited greater noise reduction than configuration 3 at frequencies above 4000 Hz (fig. 21), the advantage does not influence PWL or EPNL values noticeably. Further reduction in fan noise would be required in order to perceive any small advantage in configuration 2.

Summary of Important Conclusions

1. The splitter associated with configuration 2 resulted in a penalty of about 4 percent in thrust at rated takeoff corrected fan speed. The associated penalty in specific fuel consumption was about 6 percent. A conventional inlet could reduce the SFC loss to 4 percent. For application to any new engine development, the flow Mach number in the tailpipe would have to be decreased to minimize these losses.

2. At the maximum noise aft angle of 120° on a 114-m (375-ft) sideline at approach power, a reduction of 3.0 PNdB was shown by configuration 1. A reduction of 7.5 PNdB was credited to configuration 2, and 7.0 PNdB to configuration 3.

3. The turbine tones were suppressed somewhat by configurations 1 and 3. Configuration 2, as it should have, did the best job in suppressing the turbine tones.

4. The use of a coplanar nozzle allows more accurate measurement of tones emanating from the core without the usual "haystacking" effect of the mixing zone produced by a more conventional short fan nozzle.

5. The sound reduction level determined with the tailpipe probes was essentially in agreement with the far-field sound pressure level data.

6. In the comparison of 1/3-octave-band predicted noise reduction with the far-field data at the maximum noise aft angle of 120°, configuration 3 exceeded the design goal and, in fact, produced almost as much acoustic suppression on a PNdB basis as did configuration 2, without any aerodynamic performance loss. Configuration 2 did give substantially larger suppression of the higher frequency sound including turbine tones as it was designed to do; however, the reduction at these frequencies did not contribute appreciably to reducing the PWL level due to the encroachment of the fan noise floor.

7. Time histories of approach flyover noise indicate that a reduction of 0.5 EPNdB was achieved by configuration 1. Configurations 2 and 3 fave reductions of about 3 EPNdB.

Appendix A

Details of Design Method

The aerodynamic design of the tailpipe with the splitter installation was the result of an iterative analysis using the streamtube curvature computer program[10]. The design objectives were to conform to the geometric constraints and to minimize loads and losses associated with the splitter.

The estimated hot nozzle contour without the splitter was first analyzed with "STC" (Streamtube Calculation Program). The program utilized inlet total pressure and temperature profiles. A splitter was then placed in the stream so that it was alined with the no-splitter streamline pattern. Tentative leading and trailing contours were placed on the center section so that the leading and trailing points were along the same streamline. This was done to avoid having to iterate in STC to find the correct flow split and to minimize axial forces. Several contours were tried in obtaining a smooth Mach number distribution. The NASA-1/ellipse contour was finally chosen.

Using the Mach number distribution from STC, the boundary layer displacement thickness was calculated and added to the hard contour. This new contour was then run through STC to obtain final Mach distribution. These distributions were then used in a boundary layer program to calculate friction drag and separation function (Modified Stratford separation function[11-13]. Separation was definitely not indicated whether on the upper leading edge or the trailing contour. The critical value of F(x) was just being reached at the trailing edge.

Total pressure loss due to friction was obtained by adjusting drag values calculated by the boundary layer program in order to account for the increased drag of acoustically treated surfaces. The procedure was to increase drag calculated in the program by the ratio $0.375 \times (A_{treated}/A_{total})$ for each flow surface. Losses due to support struts were determined by the method of Ref. 14. Eight NASA-0015 struts were assumed. Calculated losses ($\%\Delta P_T/P_T$) at takeoff are summarized in the following table

Area at station 8.0, cm^2	4194	5484
Wall and splitter friction	0.680	0.840
Strut profile and friction	.012	.017
Strut interference	.018	.025
Total	0.710	0.882
Add 10% for turns, gaps, etc.	.78	.97

It should be noted that all of the above results are, for all practical purposes, independent of strut location.

Appendix B

Engine Hardware Design and Fabrication

The engine hardware utilized in this program consisted of three acoustic configurations plus a baseline hardwall configuration. The baseline hardwall configuration and configuration 1 have been previously reported in Refs. 1 and 2 and will not be discussed here. Configurations 2 and 3 were essentially the same wall hardware, with and without the acoustic splitter. Early in the design phase it was clear that the acoustic splitter was the most difficult part to be designed. Also, the previous experience in generating configuration 1 hardware could be applied to the new design.

Basically the walls consisted of single layer honeycomb sandwich conical structures furnace brazed into a single conical piece. Each piece was bolted together with sufficient body-bound (interference fit) bolts to ensure structural rigidity. A complete structural, thermal, and vibratory analysis was performed. The analysis considered gas loading, maneuver loading, and stress due to thermal gradients through the honeycomb thickness. Of the three, thermal gradients was the primary stress contributor. Finally, a local buckling failure analysis was performed.

For the acoustic splitter, analysis was performed with special emphasis on the mounting struts attaching the acoustic splitter to the wall. Eight equally spaced radial airfoil shaped struts were selected with the struts tilted forward from the inner circumference to the leading edge of the acoustic splitter as shown in Fig. 4. This strut configuration was selected because it minimized thermal stresses without complicating the fabrication procedure. The aerodynamic leading edge of the splitter was hollowed out to reduce weight and thermal stress. Also a significant weight reduction was achieved by maintaining honeycomb structure to the trailing edge.

The entire structure, including face sheets and the thin-foil resistance-welded honeycomb core, was fabricated from Inconel 625 alloy. This nickel-base alloy has very good high temperature strength in the 1000° F range and has excellent formability. The braze alloy, AMS 4777, was selected as the high temperature (1900° F range) brazing alloy because of its compatibility with Inconel 625, its ability to be welded after brazing, and its ability to bridge small gaps as well as create reasonably large fillets.

The technology for forming, assembling, and brazing complex high temperature alloy honeycomb sandwich structures is well established in several companies within the United States. Each company has different techniques, varies its approach, but the outcome is the same - a continuous, homogeneous sandwich structure. The most significant aspects of producing high quality brazed honeycomb sandwich structure was the utilization of manufacturing procedures which paid attention to cleanliness as well as precision process control in the production of each component. This was followed by careful inspection of the brazing operation by X-ray techniques and "coin-tapping" to ensure that there were no defective braze areas. Finally with each honeycomb sandwich to be furnace brazed, an identical sandwich test specimen was included for flatwise tensile tests to assure that the brazing cycle produced a quality assembly.

References

1. Clemons, A., Hehman, H., and Radecki, K., "Quiet Engine Program: Turbine Noise Suppression. Volume 1: General Treatment Evaluation and Measurement Techniques", General Electric Co., Cincinnati, Oh., P73AEG443-Vol-1, Dec. 1973; also NASA CR-134499.

2. Clemons, A., Hehmann, H., and Radecki, K., "Quiet Engine Program: Turbine Noise Suppression. Volume 2: Treatment Selection, Installation, and Test Results", General Electric Co., Cincinnati, Oh., R73AEG443-Vol-2, Dec. 1973; also NASA CR-134586.

3. Kazin, S. B. and Pass, J. E., "NASA/GE Quiet Engine C Acoustic Test Results", General Electric Co., Evendale, Oh., R73AEG364, Apr. 1974.

4. Bloomer, H. E. and Schaefer, J. W., "Aerodynamic and Accustic Performance of a Contracting Cowl High Throat Mach Number Inlet Installed on NASA Quiet Engine C", AIAA Paper 76-540, Palo Alto, Calif., 1976.

5. "DC-9 Flight Demonstration Program with Refaned JT8D Engines. Volume 4: Flyover Noise", Douglas Aircraft Co., Inc., Long Beach, Calif., MDC-J4518-Vol-4, Jul. 1975; also NASA CR-134860.

6. Bilwakesh, K. R. et al., "Core Engine Noise Control Program. Volume 3: Prediction Methods", General Electric Co. (AD-A013131/8; FAA-RD-74-125-Vol-3), Cincinnati, Oh., Aug. 1974.

7. Minner, G. L. and Rice, E. J., "Computer Method for Design of Acoustic Liners for Turbofan Engines", NASA TM X-3317, Oct. 1976.

8. Montegani, F. J., "Some Propulsion System Noise Data Handling Conventions and Computer Programs Used at the Lewis Research Center", NASA TM X-3013, Mar. 1974.

9. Stone, J. R., "Interim Prediction Method for Jet Noise", NASA TM X-71618, 1975.

10. Keith, J. S. et al., "Analytical Method for Predicting the Pressure Distribution About a Nacelle at Transonic Speeds". NASA CR-2217, Jul. 1973.

11. Stratford, B. S., "The Prediction of Separation of the Turbulent Boundary Layer", Journal of Fluid Mechanics, Vol. 5, Pt. 1, Jan. 1959, pp. 1-16.

12. Cebeci, T., Mosinskis, G. J., and Smith, A. M. O., "Calculation of Separation Points in Incompressible Turbulent Flows", Journal of Aircraft, Vol. 9, No. 9, Sept. 1972, pp. 618-624.

13. Lahti, D. J., "The Prediction of Turbulent Boundary Layer Separation Using a Modified Form of the Stratford Method", General Electric Co., Evendale, Oh., Tech Memo 72-618, Oct. 1972.

14. Wagenknecht, C. D., "GE13/CTOL Demo Engine Frame Strut Loss Analytical Method", General Electric Co., Evendale, Oh., ESAD Tech. Brief 71014, Aug. 1974.

15. "Definitions and Procedures for Computing the Perceived Noise Level of Aircraft Noise", Aerospace Recommended Procedure 865A, SAE, Aug. 1969.

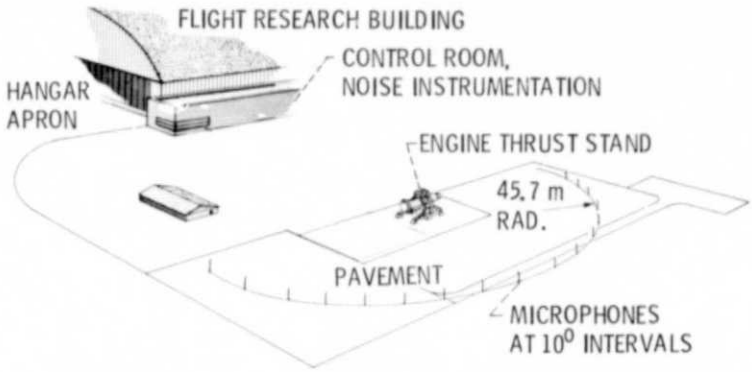

Figure 1. - Engine Noise Test Facility plot plan showing thrust stand, microphone array, control and noise instrumentation rooms.

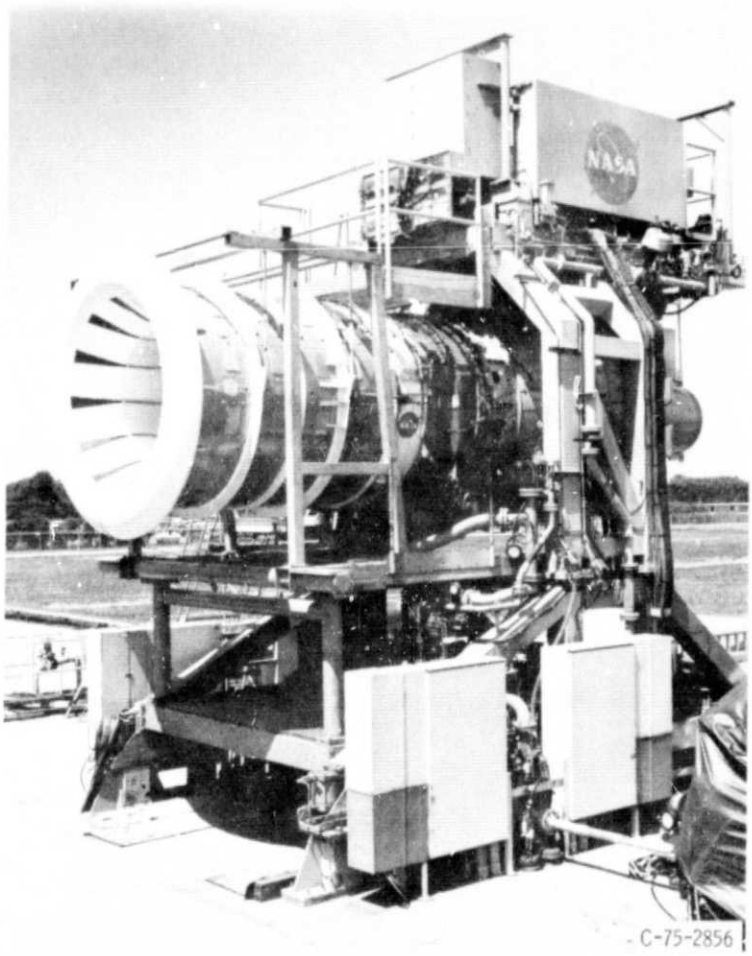

Figure 2. - Engine noise test facility at Lewis Research Center. View of Quiet Engine "C" installation showing the sonic inlet used to quiet inlet fan noise.

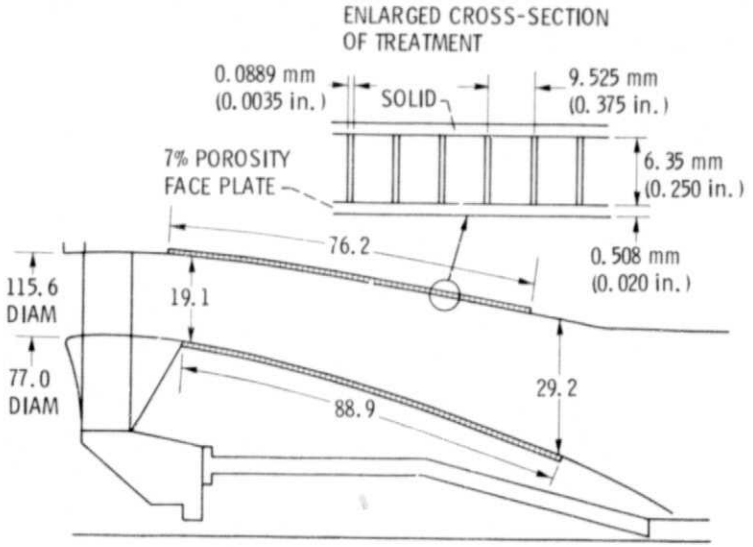

Figure 4 - Contractor-designed core suppressor for NASA Quiet Engine "C". (Configuration 1.)

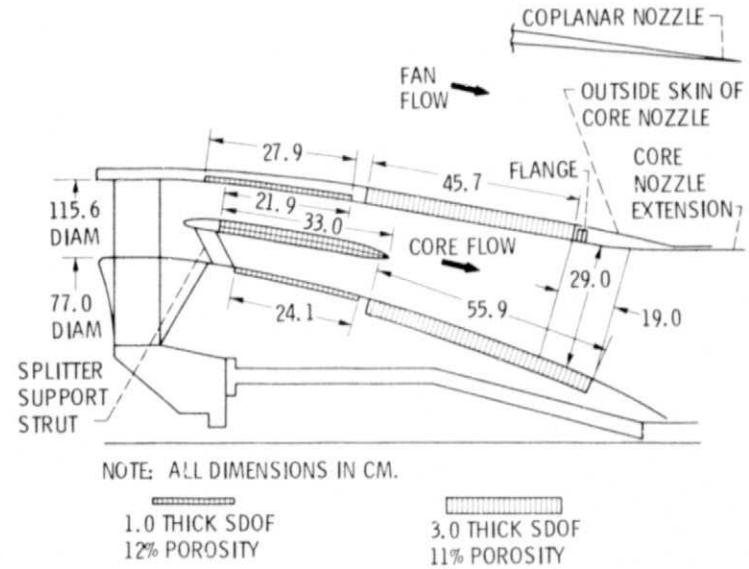

(a) SCHEMATIC OF CONFIGURATION 2 (WITHOUT SPLITTER, CONFIGURATION 3).

Figure 4. - NASA designed core suppressor for NASA Quiet Engine "C".

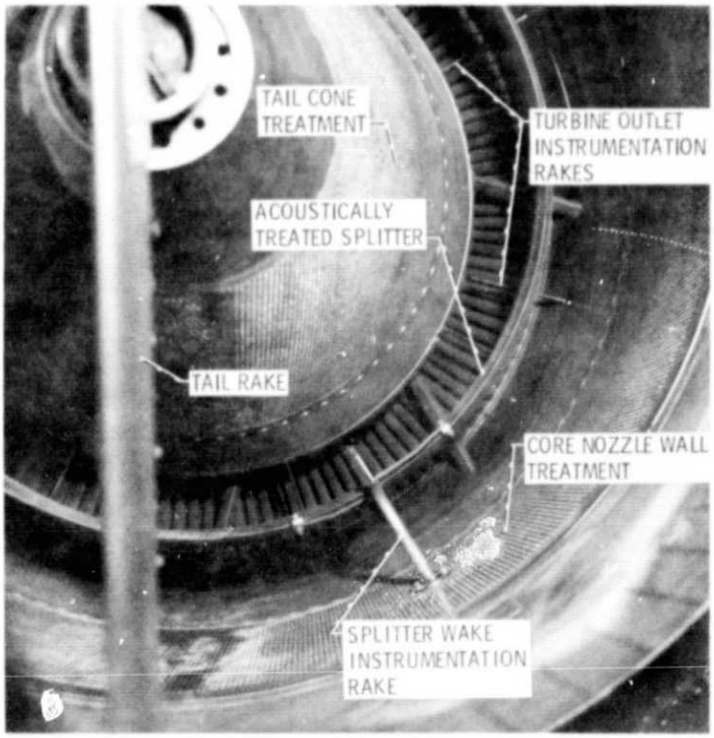

(b) PHOTOGRAPH OF CONFIGURATION 2 SHOWING SPLITTER AND AERODYNAMIC INSTRUMENTATION.

Figure 4. - Concluded.

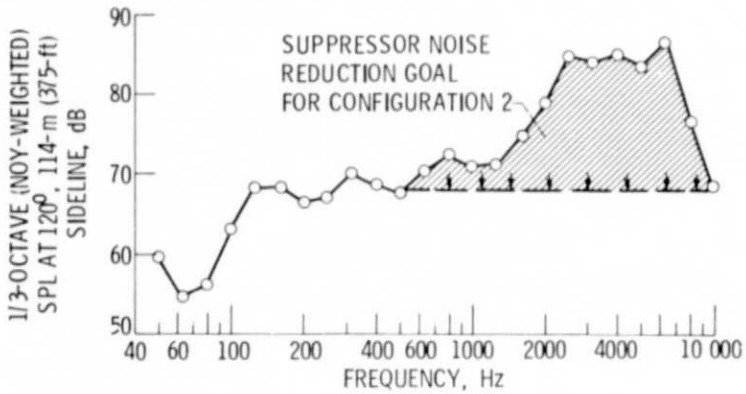

Figure 5. - NOY-weighted 1/3-octave-band spectrum far-field baseline data showing noise reduction goal. 120° microphone extrapolated to 114-m sideline at approach power.

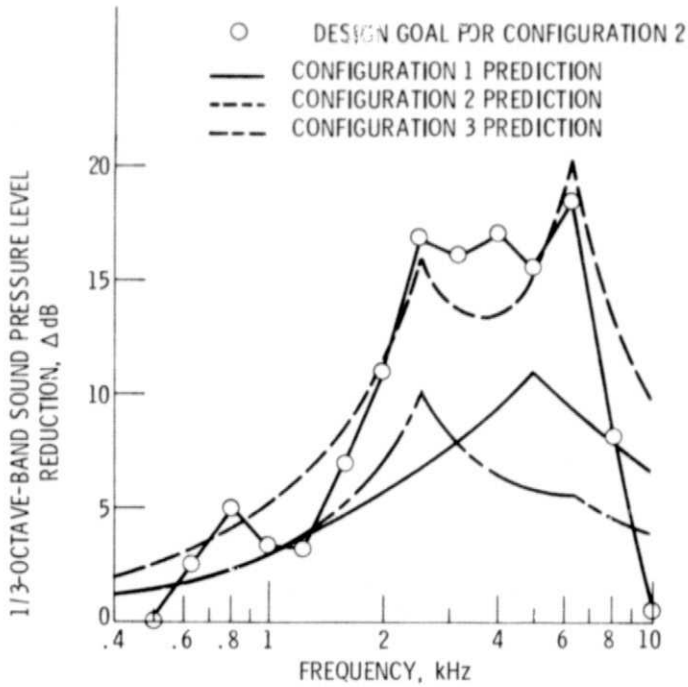

Figure 6. - Comparison of design suppression predictions for all configurations at peak noise aft angle of 120° and approach power setting using method of reference 7.

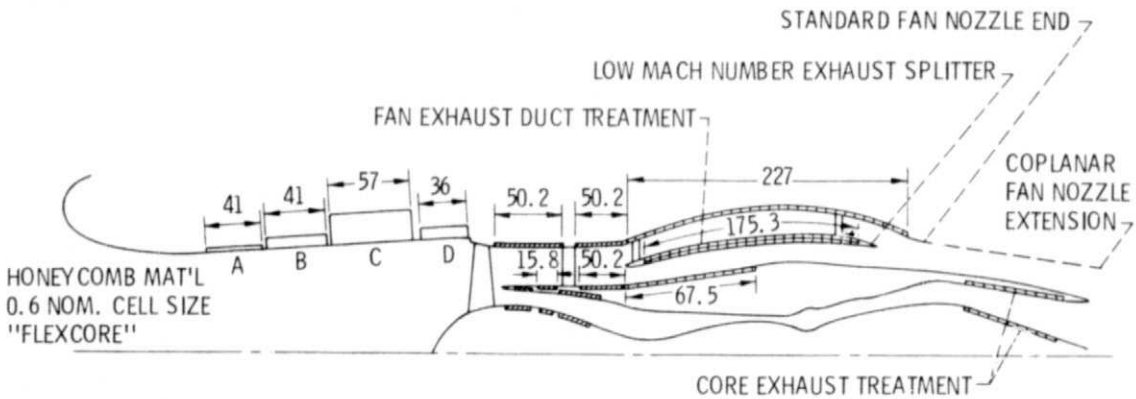

TAKEOFF SONIC INLET TREATMENT DETAILS

	B'KING DEPTH	FACING SHEET		
		THICKNESS	HOLE DIAM.	% OPEN
A	0.76	0.08	0.14	7.3
B	2.54	.08	.14	10.0
C	7.19	.08	.14	2.5
D	2.79	.13	.13	7.0

NOTE: ALL DIMENSIONS ARE IN CM.

FAN DUCT AND CORE TREATMENT DETAILS

- 2.54 THICK MDOF 10% POROSITY
- 0.64 THICK SDOF 7% POROSITY
- 2.54 THICK SCOTTFELT

Figure 7. - Quiet Engine "C", cross section of fully suppressed configuration showing core suppressor configuration 1 installed.

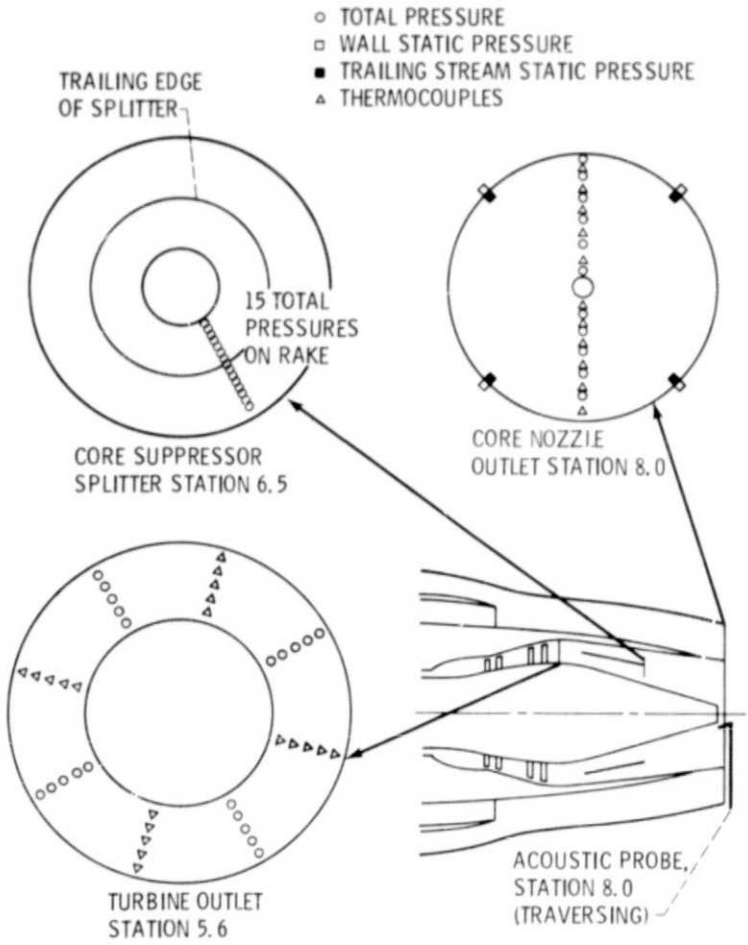

Figure 8. - Core suppressor instrumentation schematic.

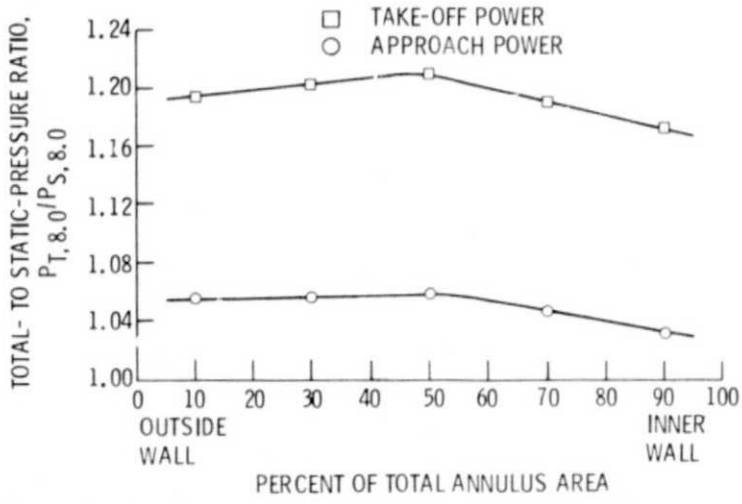

Figure 9. - Total- to static-pressure ratio at turbine outlet station.

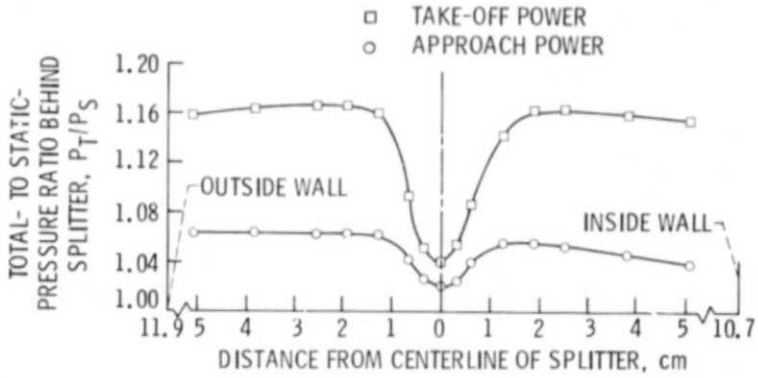

Figure 10. - Total- to static-pressure ratio behind splitter of configuration 2.

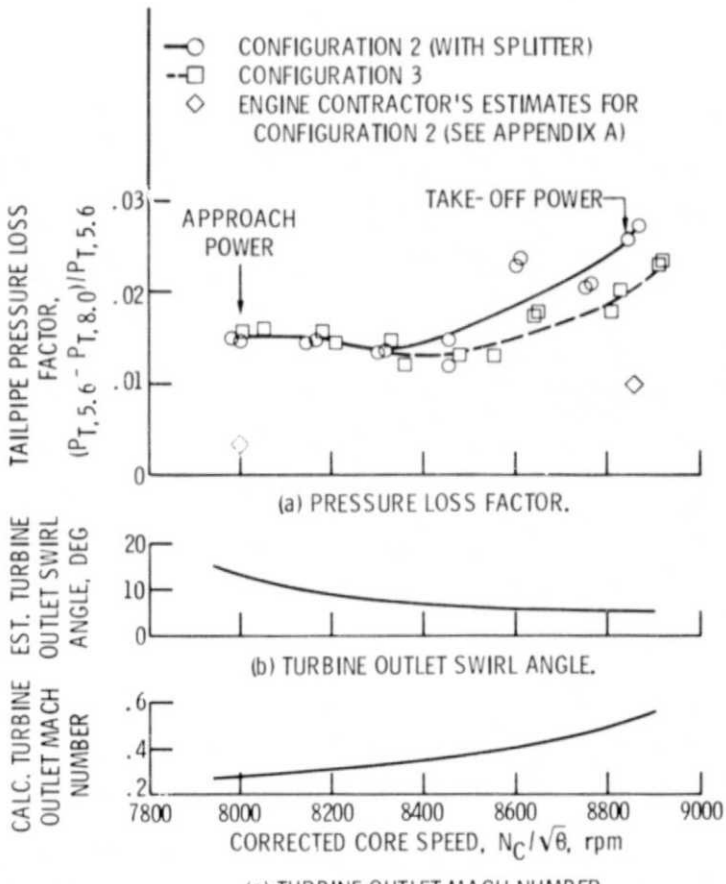

Figure 11. - Comparison of engine parameters for configurations with and without splitter over range of corrected core engine speeds.

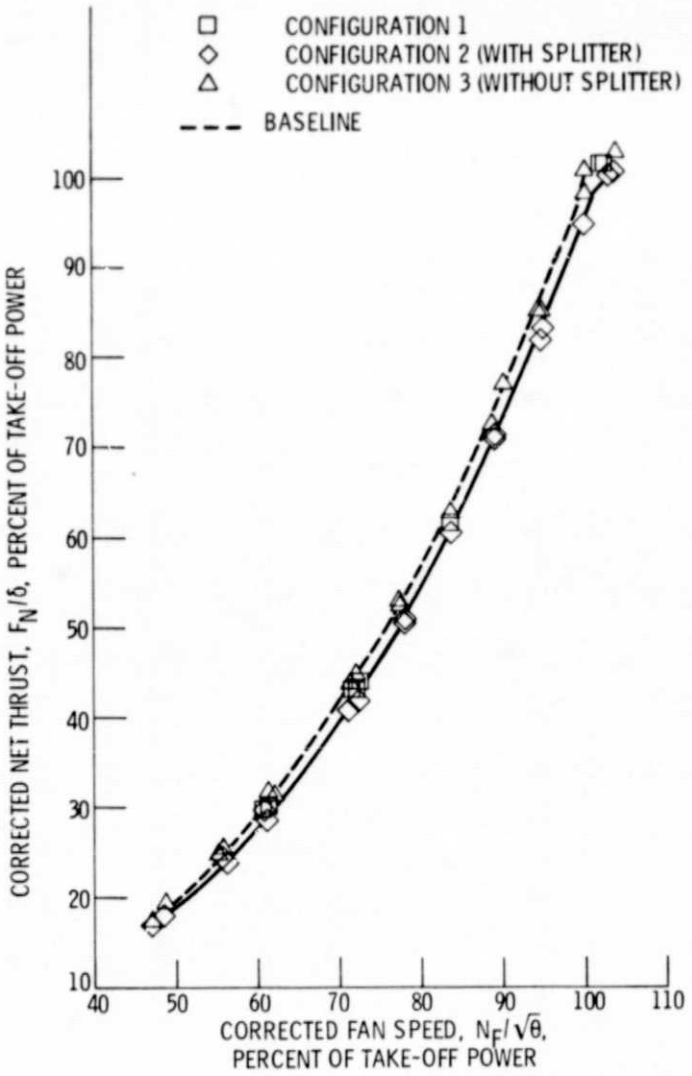

Figure 12. - Comparison of variation of corrected net thrust with corrected fan speed for configurations with and without core splitters.

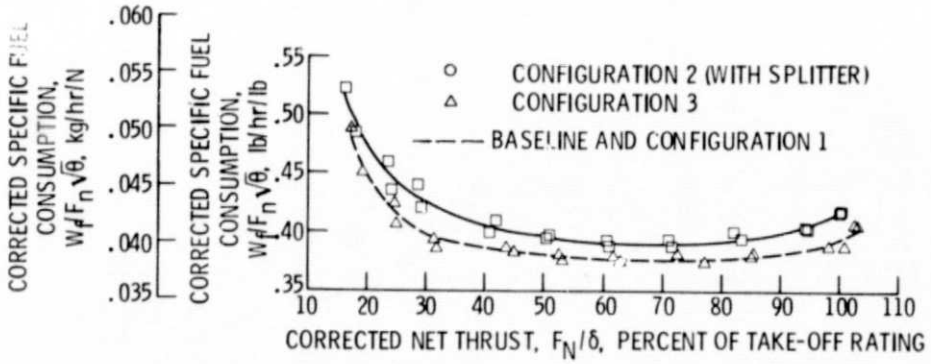

Figure 13. - Comparison of variation of corrected specific fuel consumption with corrected net thrust for configurations with and without splitter.

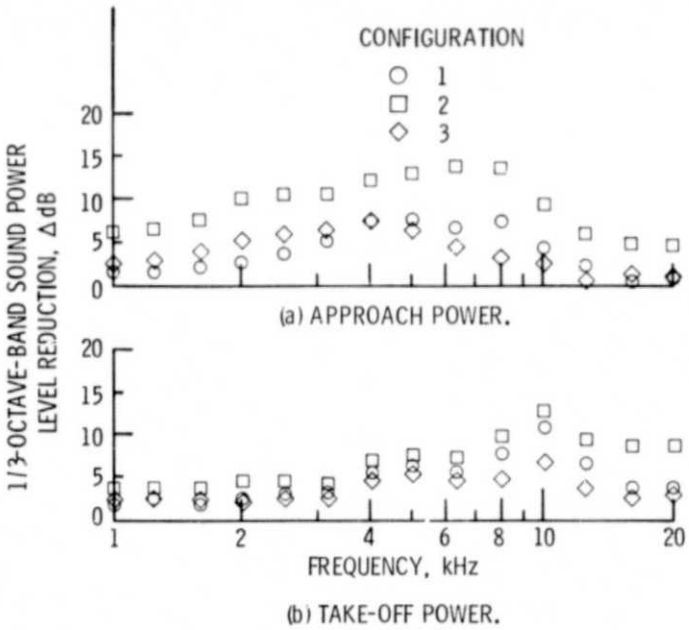

Figure 14. - Sound power level reduction over treated surface of suppressor configurations compared to baseline (hard surface) configuration. In-duct acoustic probe data.

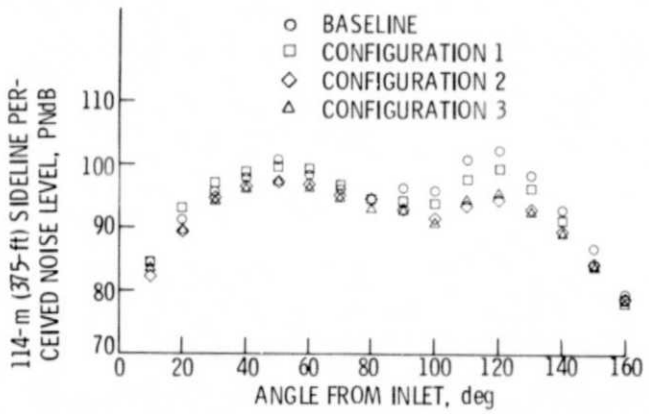

Figure 15. - Perceived noise directivities at approach power for all configurations.

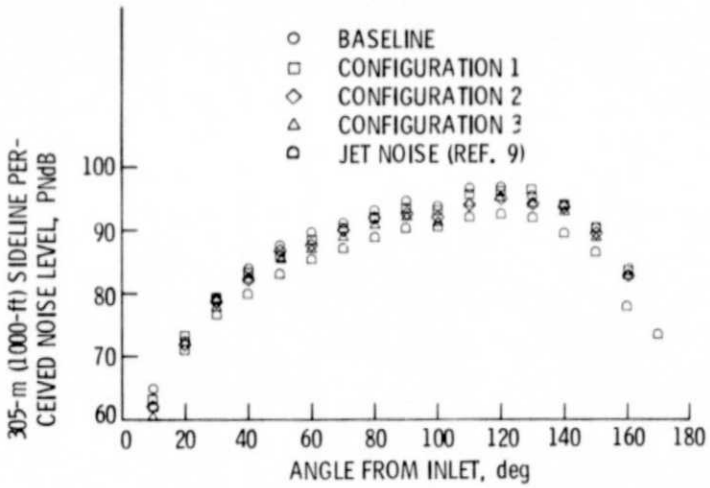

Figure 16. - Perceived noise level directivities at take-off power for all configurations.

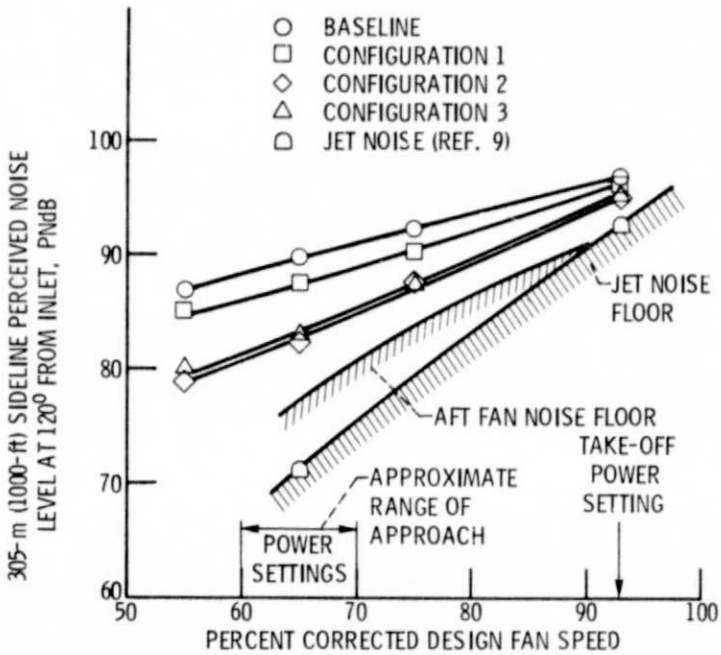

Figure 17. - Comparison of perceived noise level at peak noise aft angle of 120° over range of engine power settings.

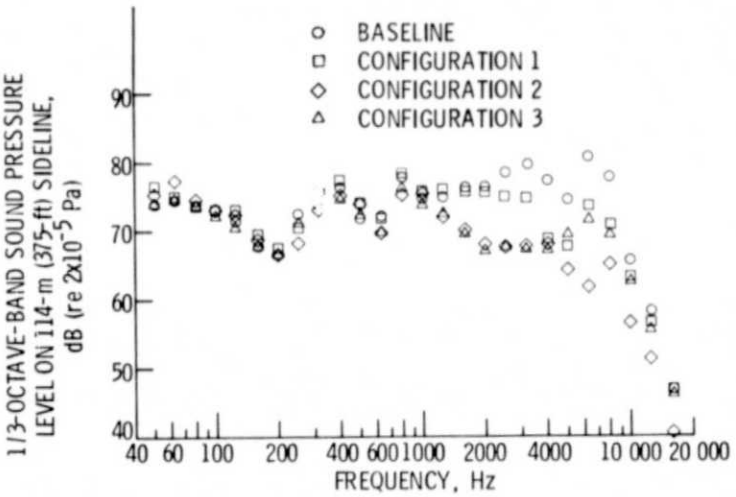

Figure 18. - Comparison of 1/3-octave spectra for baseline and suppressed configurations. Far-field 120° microphone data. Approach power. Data corrected to standard day of 59° F and 70 percent relative humidity.

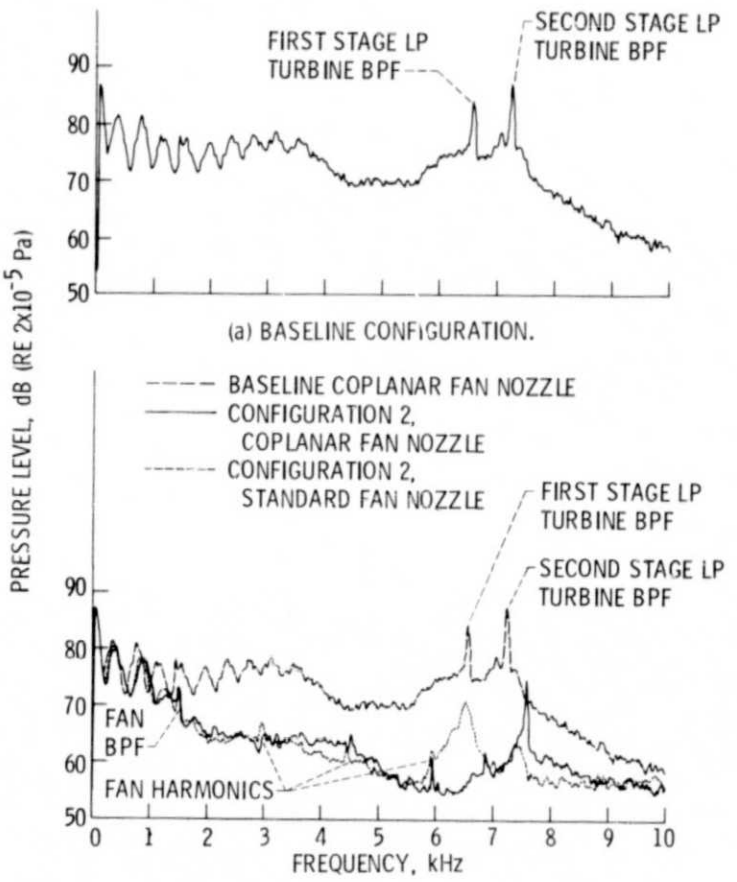

Figure 19. - Approach power narrow-band spectra at peak noise aft angle of 120°; 45.7 m; filter bandwidth, 30 Hz.

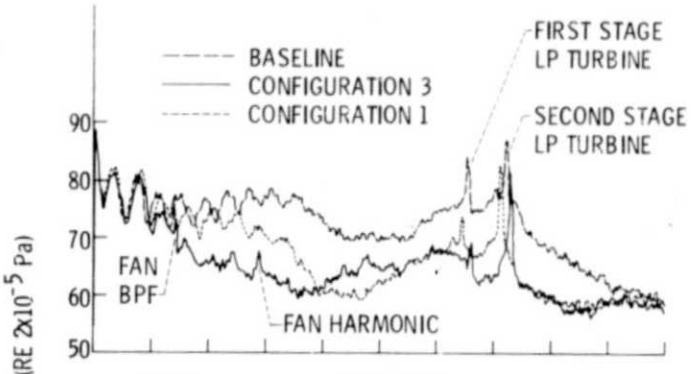

(c) COMPARISON OF CONFIGURATIONS 1 AND 3.

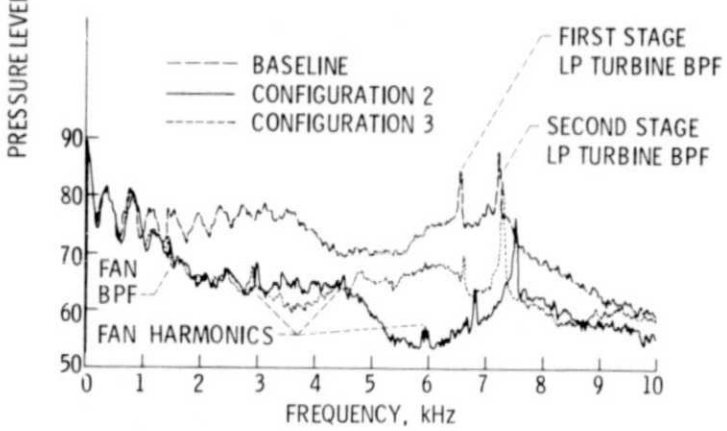

(d) EFFECT OF SPLITTER.

Figure 19. - Concluded.

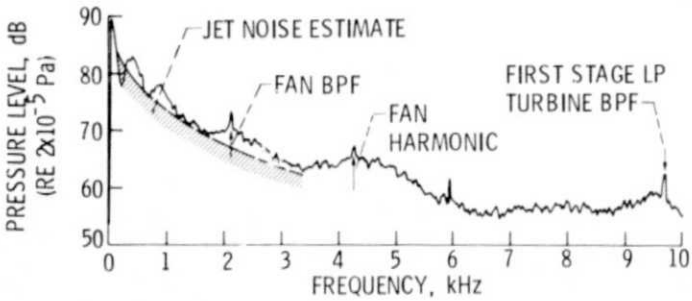

Figure 20. - Take-off power narrow band spectra. Configuration 2 with coplanar fan nozzle. 120° microphone data at 45.7 m. Filter bandwidth, 30 Hz.

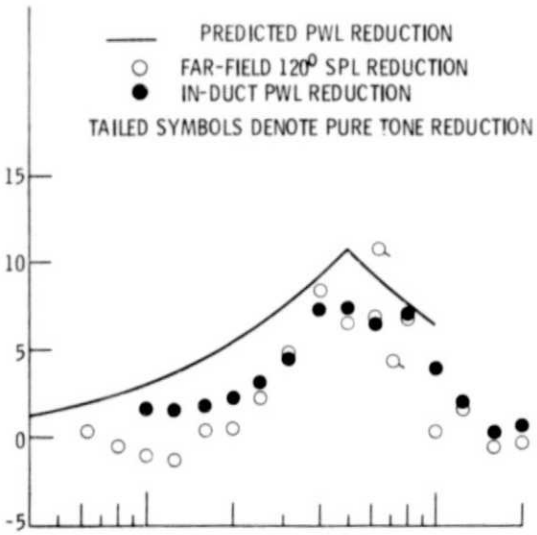

(a) CONFIGURATION 1.

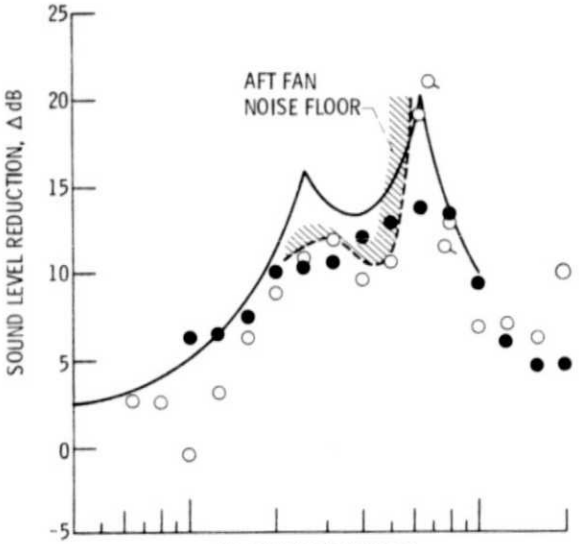

(b) CONFIGURATION 2.

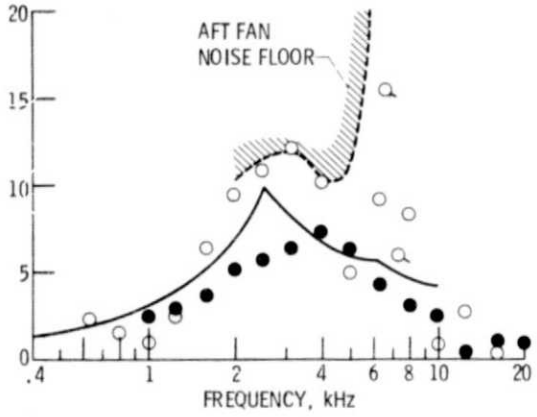

(c) CONFIGURATION 3.

Figure 21. - Comparison of predicted, far-field (120°) and in-duct sound level reduction characteristics. Approach power design point.

		EFFECTIVE PERCEIVED NOISE, dB	AVERAGE PERCEIVED NOISE LEVEL TONE CORRECTED
△	BASELINE	103.2	105.6
○	CONFIGURATION 1	102.8	104
□	CONFIGURATION 2	100.9	102.1
◇	CONFIGURATION 3	100	100.9

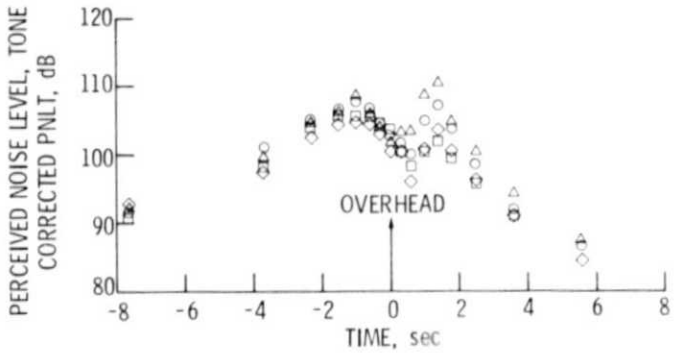

Figure 22. - Approach time histories (flyover noise) for baseline and suppressor configurations of tone corrected PNL's.

NASA-Lewis